International Journal of Nanomedicine

Dovepress
open access to scientific and medical research

Open Access Full Text Article

ORIGINAL RESEARCH

Preparation of Fe_3O_4 magnetic nanoparticles coated with gallic acid for drug delivery

Dena Dorniani[1]
Mohd Zobir Bin Hussein[1,2]
Aminu Umar Kura[3]
Sharida Fakurazi[3]
Abdul Halim Shaari[4]
Zalinah Ahmad[5]

[1]Chemistry Department, Faculty of Science, [2]Advanced Materials and Nanotechnology Laboratory, Institute of Advanced Technology, [3]Vaccines and Immunotherapeutics Laboratory, [4]Physics Department, Faculty of Science, [5]Chemical Pathology Unit, Department of Pathology, Faculty of Medicine and Health Sciences, Universiti Putra Malaysia, Selangor, Malaysia

Background and methods: Magnetic iron oxide nanoparticles were prepared using a sonochemical method under atmospheric conditions at a Fe^{2+} to Fe^{3+} molar ratio of 1:2. The iron oxide nanoparticles were subsequently coated with chitosan and gallic acid to produce a core-shell structure.

Results: X-ray diffraction demonstrated that the magnetic nanoparticles were pure Fe_3O_4 with a cubic inverse spinel structure. Transmission electron microscopy showed that the Fe_3O_4 nanoparticles were of spherical shape with a mean diameter of 11 nm, compared with 13 nm for the iron oxide-chitosan-gallic acid (FCG) nanocarriers.

Conclusion: The magnetic nanocarrier enhanced the thermal stability of the drug, gallic acid. Release of the active drug from the FCG nanocarrier was found to occur in a controlled manner. The gallic acid and FCG nanoparticles were not toxic in a normal human fibroblast (3T3) line, and anticancer activity was higher in HT29 than MCF7 cell lines.

Keywords: magnetic nanoparticles, chitosan, superparamagnetic, controlled-release, gallic acid, drug delivery

Introduction

Nanotechnology is now widely used throughout the pharmaceutical industry, medicine, electronics, robotics, and tissue engineering. The use of nanoparticles in the development of delivery systems for small molecules, DNA, RNA, plasmids, and proteins has been studied extensively over the past decade. Nanoparticles have also been used to deliver drugs to target tissues and to increase stability against degradation by enzymes.

One of these nanoparticles is the superparamagnetic nanoparticle, which can be manipulated by an external magnetic field to lead it to the target tissue.[1] Superparamagnetic nanoparticles are relatively safe and can also be used as contrast agents in magnetic resonance imaging. The nanostructure is based on an inorganic core of iron oxide, such as magnetite (Fe_3O_4), maghemite (γ-Fe_2O_3), or other insoluble ferrites coated with a polymer such as dextran, chitosan, poly(ethylenimine) (PEI), poly(ethylene glycol) (PEG), or copolymers, such as (PEI-PEG-chitosan).[2] Magnetite is an important type of magnetic material, having a cubic inverse spinel structure, and has been the subject of increasing attention because of its use in magnetic recording tape,[3] ferrofluid,[4] catalysts,[5] and biomedical applications, such as magnetic resonance,[6–8] bioseparation,[9–11] drug targeting,[12,13] and hyperthermia.[14–17] Magnetic nanoparticles of iron oxide have been studied extensively in various applications, such as controlled magnetic transportation of anticancer drugs as well as generation of hyperthermia.[18–20]

Correspondence: Mohd Zobir Bin Hussein
Chemistry Department, Faculty of Science, Universiti Putra Malaysia, 43400 Serdang, Selangor, Malaysia
Tel +603 8946 6801
Fax +603 8943 5380
Email mzobir@science.upm.edu.my

submit your manuscript | www.dovepress.com
Dovepress
http://dx.doi.org/10.2147/IJN.S35746

The progress of systems for targeted drug delivery has been reviewed by Moghimi et al.[21] Previous study on in vitro evaluation of the characteristics of nanoparticles found that some of the most important factors determining nanoparticle cytotoxicity were particle size, particle morphology, surface area, and particle reactivity in solution.[22]

Researchers have synthesized magnetite particles coated with dextran to enhance the capture of magnetite nanoparticles in capillary tissue.[23] Carriers were prepared from poorly soluble drugs by grafting hydrophobic moieties, hydrophilic moieties, and glycidol.[24] Novel magnetic iron oxide nanoparticles were also coated with PEI-g-PEG for potential biomedical application.

Lung cancer is one of the most common cancers in the world. Gallic acid has a wide range of biological applications and is distributed in a variety of fruits, plants, and foods. A polyhydroxylphenolic compound, gallic acid has antiviral, antibacterial, antimelanogenic, and anticancer activity in a range of cells. Cell cytotoxicity and adhesion studies have shown that superparamagnetic iron oxide nanoparticles are toxic to human dermal fibroblasts, and their internalization results in disruption of the organization of the cytoskeleton in these cells.[25] The objective of this work was to synthesize a nanocarrier comprised of ferrite nanoparticles coated with chitosan and gallic acid (FCG) for active drug delivery and specific cell targeting in normal human fibroblasts (3T3) and in cancer cell lines.

Materials and methods

Materials

All the materials used in this study were of analytical grade and required no further purification. Iron (II) chloride tetrahydrate ($FeCl_2 \cdot 4H_2O \geq 99\%$) and iron (III) chloride hexahydrate ($FeCl_3 \cdot 6H_2O$, 99%) were purchased from Merck KGaA (Darmstadt, Germany). Chitosan (low molecular weight, deacetylation 75%–85%) was sourced as a raw material for Sigma-Aldrich (St Louis, MO). Gallic acid of 97% purity was also obtained from Sigma-Aldrich. Aqueous acetic acid solution 99.8% was used as a solvent for chitosan, purchased from Hamburg Industries Inc, Hamburg, Germany. All the aqueous solutions were prepared using distilled deionized water (18.2 $M \cdot \Omega\ cm^{-1}$).

Preparation of chitosan

To prepare the Fe_3O_4-chitosan nanoparticles, chitosan was first coated onto the surface of the nanoparticles by physical absorption, and the resulting Fe_3O_4-chitosan nanoparticles were obtained.[26] Typically, 0.5 mL of acetic acid 99.8% was made up to a volume of 100 mL with deionized water, and 1 g of chitosan was added to the solution (0.5%) under vigorous mechanical stirring for 3 hours. Chitosan has a strong metal ion-chelating ability as a result of the nitrogen atom, so chitosan is a potential antioxidant based on its metal ion deactivation.[27] Gallic acid is attractive for conjugation onto chitosan because of the high reducing potential and low O–H band dissociation enthalpy of the trihydroxyl groups on the benzene ring; the possibility for the bulky group on the benzene ring of gallic acid to obstruct the intermolecular and intramolecular hydrogen bond network of chitosan; the multifunctional hydrophilicity based on the hydroxyl and carboxyl groups; the carboxylic acid group for conjugation with chitosan; and it being a natural product.[27]

In addition, chitosan can be chemisorbed onto the anionic magnetite surface and is visible as a silk-like black precipitate. It is also feasible that unbound primary amino groups, hydrogen bonding, electrostatic attraction, and hydrophobic effects may play an important role in preventing aggregation of chitosan-coated superparamagnetic iron oxide.[26]

Previous research also suggests that the scavenging mechanism of chitosan against free radicals may be related to the active hydrogen of NH_2 on the C2 and OH groups at the C6 position. Therefore, gallic acid can interact with macromolecular chitosan radicals generated by redox pair systems, particularly NH_2 at the C2 position and OH groups at the C6 position.[28]

Preparation of magnetic nanoparticles and coating procedure

Because the surface of the iron oxide is negatively charged, it has an affinity toward amine groups of chitosan. Therefore, protonated chitosan could be coated on the magnetite nanoparticles by electrostatic interaction and chemical reaction through epichlorohydrin crosslinking.[29] The amino groups present on the chitosan can be used for further functionalization with other functional groups from the drug moiety with specific binding sites.[26]

Iron oxide nanoparticles were prepared by dissolving 2.43 g ferrous chloride tetrahydrate ($FeCl_2 \cdot 4H_2O$), 0.99 g ferric chloride hexahydrate ($FeCl_3 \cdot 6H_2O$), and 80 mL of deionized water in the presence of 6 mL ammonia hydroxide (25% by mass). The solution was exposed to ultrasonic irradiation (20 kHz) for one hour. The precipitate was then centrifuged and washed three times, after which the washed precipitate was dispersed in 100 mL of deionized water and mixed with 10 mL of chitosan (1%) and 10 mL of gallic

acid (4%) dissolved in water. The mixture was then stirred for 24 hours. Next, the black precipitate was collected by permanent magnet and dried in an oven. It is obvious that changing the pH can affect the superparamagnetic performance and grain size of iron oxide nanoparticles. Previous study has shown that when pH is <11, the grain size is slightly decreased with increasing pH values; however, when pH is >11, the grain size stays almost unchanged.[30] A previous study suggested that the optimum pH to produce pure magnetic nanoparticles must be within the range of 9.7–10.6. pH values below 8.5 may cause side reactions, namely production of goethite maghamite.[31]

MTT cytotoxicity assay

MCF-7, 3T3, and HT29 cell lines were obtained from the American Tissue Culture Collection (Manassas, VA) and maintained in RPMI 1640 medium supplemented with 10% fetal bovine serum, L-glutamine 15 mmol/L, penicillin 100 U/mL, and streptomycin 100 µg/mL, and incubated at 37°C in humidified 5% CO_2/95% air. For the MTT (3-(4, 5-dimethylthiazol-2-yl)-2,5-diphenyltetrazolium bromide) assay, the cells were plated into a 96-well plate at a density of 1.0×10^5 cells per well in 100 µL culture medium and allowed to attach for 24 hours. A stock solution of nanoparticles and gallic acid was prepared in dimethyl sulfoxide, and subsequently diluted in medium to obtain the desired concentration of 0.47–30 µg/mL at a final volume of 200 µL in each well. Cell viability and cytotoxicity was assessed using an MTT assay after exposure to the nanoparticles and gallic acid. Only functional mitochondrial dehydrogenase enzymes from viable cells can reduce MTT to formazan. A 20 µL aliquot of MTT solution at a concentration of 5 mg/mL was added to each well and incubated at 37°C for 3 hours. To solubilize the formazan after 3 hours of incubation, 100 µL of dimethylsulfoxide was added to each well and kept in the dark at room temperature for 30 minutes. Optical density values were measured at wavelengths of 570 nm and 630 nm using an enzyme-linked immunosorbent assay reader (Thermo Fisher Scientific Inc, Waltham, MA). Three independent experiments were carried out for each concentration of nanoparticles and gallic acid.

Characterization

Powder X-ray diffraction patterns were used to determine the crystal structure of the samples in the range of 25–70 degrees on an XRD-6000 diffractometer (Shimadzu, Tokyo, Japan) using CuK_α radiation (λ 1.5406 Å) at 40 kV and 30 mA. To study the functional groups, Fourier transform infrared spectroscopy of the materials was recorded over the range of 400–4000 cm^{-1} on a 1752X spectrophotometer (Perkin-Elmer, Waltham, MA) using the KBr disc method. Thermogravimetric analysis was carried out using a Mettler Toledo instrument in 150 µL alumina crucibles in the range of 20°C–1000°C. Scanning electron microscopy was used to observe the surface morphology of the samples using a JSM-6400 machine (JOEL, Tokyo, Japan). The mean particle size, size distribution, and morphology of the samples were obtained using a transmission electron microscope (Hitachi H-7100, Tokyo, Japan) at an accelerating voltage of 80 and 200 kV.

Controlled-release study

To evaluate the controlled-release characteristics of gallic acid coated on FCG, different anions, including Cl^-, CO_3^{2-} and PO_4^{-3}, were used. For the release study, we used two different pH levels which are similar to the pH of the stomach and the pH of the blood. Generally, the pH of the stomach varies from 1–2 to 4–5. After eating, the stomach releases proteases and hydrochloric acid to aid digestion. In itself, the acid does not aid digestion, but the proteases that cleave proteins work best in an acidic environment. Therefore, after a high-protein meal, the stomach pH may drop to as low as 1–2. However, buffer quickly raises the pH back to 3–4. After the meal has been digested, the pH of stomach returns to a resting level of about 4–5. Before food arrives, the pH of the stomach is normally 5.0–6.0. It is clear that an ideal level of pH in the blood is about 7.4, and even changing this level slightly may have fatal consequences. Therefore, release of gallic acid from nanoparticles was determined using a 0.0001 M aqueous solution of Na_2CO_3[32] and Na_3PO_4 buffered solutions of pH 4.8[33–39] and 7.4[37,38,40,41] at 37°C. The gallic acid released was measured at preset times using ultraviolet-visible spectrophotometry at 264 nm. About 21 mg of the iron oxide nanocarrier coated with chitosan and gallic acid was added to 50 mL of Na_2CO_3 and stirred for 24 hours, and the amount of gallic acid released was measured at λ_{max} 264 nm.

Results and discussion

X-ray diffraction

The X-ray diffraction patterns for the naked iron oxide nanoparticles and iron oxide nanoparticles coated with chitosan and gallic acid are shown in Figure 1. For both samples, six characteristic peaks observed at 2θ = 30.3°, 35.7°, 43.4°, 53.6°, 57.3°, and 62.9°, can be assigned as (220), (311), (400), (422), (511), and (440), respectively.

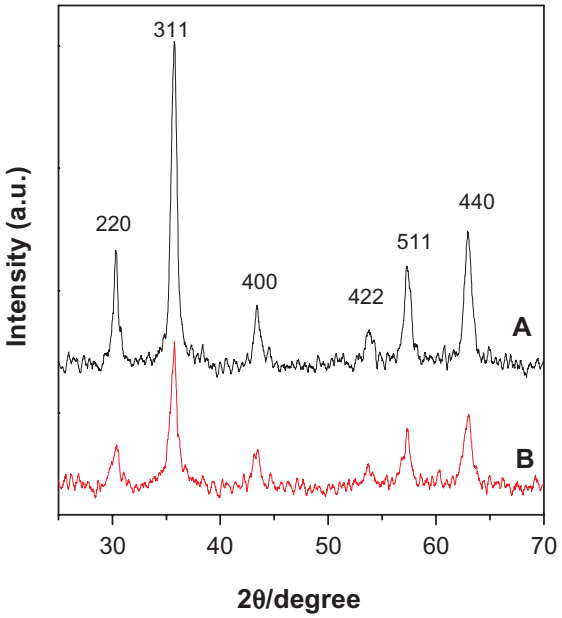

Figure 1 X-ray diffraction patterns for (**A**) pure iron oxide nanoparticles and (**B**) iron oxide nanoparticles coated with chitosan and gallic acid.

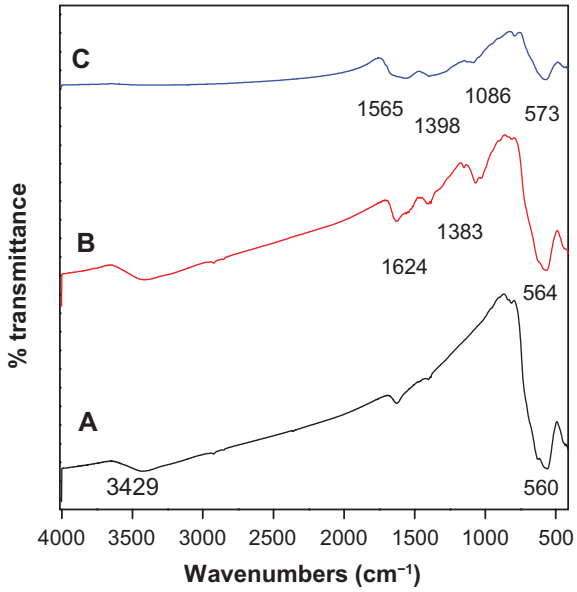

Figure 2 Fourier transform infrared spectra of (**A**) iron oxide nanoparticles, (**B**) iron oxide nanoparticles coated with chitosan, and (**C**) iron oxide nanoparticles coated with chitosan and gallic acid.

The diffraction peaks of each sample matched the diffraction peaks for pure iron oxide and revealed that the resulting magnetic nanoparticles were pure Fe_3O_4 with a cubic inverse spinel structure. It was also found that the coating process for Fe_3O_4 did not affect the phase change of iron oxide. X-ray diffraction patterns show the broad nature of the diffraction bands, indicating small particle sizes that can be quantitatively calculated according to the Debye-Scherrer equation, ie, ($D = K\lambda/\beta \cos \theta$),[42–44] which shows a relationship between peak broadening in x-ray diffraction and particle size, where D is the particle size, K is the Debye-Scherrer constant (0.89), λ is the x-ray wavelength (0.15406 nm), β is the peak width of half-maximum, and θ is the diffraction angle. Using the x-ray results and this equation, the particle size of the naked iron oxide nanoparticles and of the iron oxide nanoparticles coated with chitosan and gallic acid was calculated to be 5 nm and 9 nm, respectively.

Fourier transform infrared spectra

Figure 2 shows the Fourier transform infrared spectra of the as-synthesized Fe_3O_4 nanoparticles, Fe_3O_4 nanoparticles coated with chitosan, and Fe_3O_4 coated with chitosan and gallic acid. The peak at 3429 cm^{-1} observed in spectrum A and B relates to the —OH group. The characteristic peak of Fe_3O_4 at around 560 cm^{-1} could be observed in all of the three spectra, and relates to the Fe—O bond. Figure 2B shows the characteristic peak absorption bands observed at 1624 cm^{-1}, which can be assigned to N—H bending vibration, and the 1383 cm^{-1} peak can be assigned to —C—O stretching of the primary alcoholic group in chitosan. Also, due to the reaction of chitosan with glutaraldehyde forming a Schiff base, a sharp peak appeared at 564 cm^{-1}. In the spectrum for Fe_3O_4 coated with chitosan, compared with the spectrum of iron oxide coated with chitosan and gallic acid nanoparticles, the 1624 cm^{-1} peak for N—H bending vibration shifted to 1565 cm^{-1} and the Fe—O bond shifted to 573 cm^{-1}. It could be seen that chitosan and gallic acid were coated onto the Fe_3O_4 nanoparticles successfully, and the negative charges on the iron oxide surface had an affinity for chitosan and protonated it. Thus, the coating occurred by electrostatic interaction and a chemical reaction via glutaraldehyde cross-linking.

Magnetic properties

The magnetic properties of iron oxide nanoparticles and iron oxide nanoparticles coated with chitosan and gallic acid were characterized by vibrating sample magnetometry. Figure 3 shows the hysteresis loops as a function of the magnetic field at room temperature. The magnetic parameters, including saturation magnetization and remnant magnetization, are shown in Table 1. The saturation magnetization of the iron oxide nanoparticles core-shelled by chitosan and gallic acid was about 26.074 emu/g, while the naked iron oxide was about 29.091 emu/g. The decrease in saturation magnetization

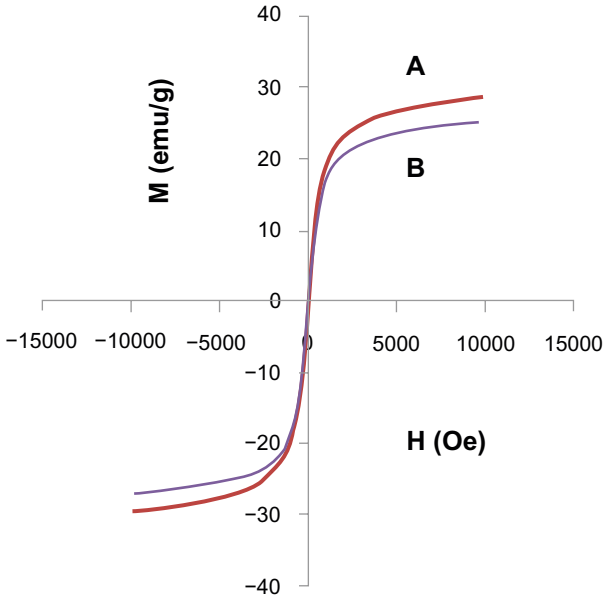

Figure 3 Magnetization plots of (**A**) iron oxide magnetic nanoparticles and (**B**) iron oxide nanoparticles coated with chitosan and gallic acid.

was most likely due to the existence of coated materials and impurities on the surface of the magnetic nanoparticles.[45] According to the vibrating sample magnetometry results, the nanoparticles showed superparamagnetic behavior, ie, they did not retain any magnetism after removal of the magnetic field. High magnetization and superparamagnetic properties are highly sought after for biomedical applications because the larger magnetic particles form aggregates after exposure to a magnetic field.

Thermogravimetric analysis

Thermogravimetric analysis is one of the most important techniques used to determine thermal stability and phyicochemical properties of compound by percent weight loss. Thermogravimetric-derivative thermogravimetric analysis of gallic acid and iron oxide nanoparticles coated with chitosan and gallic acid was performed under atmospheric conditions. The thermogravimetric analysis curves for gallic acid show the first stage of weight loss at 86°C (8.8%), which might have occurred because of removal of crystalline water (Figure 4A).

Table 1 Magnetic properties of Fe_3O_4 magnetic nanoparticles and FCG

Samples	Ms (emu/g)	Mr (emu/g)
Fe_3O_4	29.091	1.098
FCG	26.074	1.795

Abbreviations: FCG, iron oxide nanoparticles coated with chitosan and gallic acid; Ms, saturation magnetization; Mr, remnant magnetization.

The differential thermogravimetric curves indicate the onset of weight loss at 264°C (41.0%) and 325°C (22.5%). The curved shape of the thermogravimetric-derivative thermogravimetric thermograms changed due to the coating (Figure 4B). The first weight loss at 66.5°C corresponded to the apparent minimum removal of free and chemically adsorbed water. The onset of degradation of Fe_3O_4 and dehydroxylation of gallic acid occurred at 227°C, which is higher than the decomposition temperature of pure gallic acid. The slow mass reduction (25.7%) occurring at 811°C is due to decomposition of chitosan. The temperature range in Figure 4B is higher than that for the pure free gallic acid (Figure 4A), indicating that the magnetic nanocarrier enhanced the thermal stability of gallic acid.

Surface properties

The surface morphology of the as-synthesized magnetite nanoparticles was observed by scanning electron microscopy. Figure 5 shows typical images of naked iron oxide nanoparticles and iron oxide nanoparticles coated with chitosan and gallic acid. Figure 5B shows that the iron oxide nanoparticles had a spherical shape, and were transformed into an agglomerated structure without any specific shape, as shown in Figure 5C and D, when coating of iron oxide nanoparticles took place.

Determination of mean size and size distribution properties

Transmission electron microscopy of the magnetic iron oxide nanoparticles and iron oxide nanoparticles coated with chitosan and gallic acid was performed to determine the shape, size, and uniformity of the particles under optimum conditions. The particle size and size distribution of the particles was calculated using Image analysis software from at least 200 particles chosen randomly from all synthesized samples. The as-prepared iron oxide nanoparticles were predominantly spherical, which was confirmed by field emission scanning electron microscopy. Figure 6 shows that these particles had a very small size of around 11–13 nm in diameter, with a narrow size distribution. The average size of the magnetic nanoparticles was 11.4 ± 2.2 nm, whereas the mean size of the iron oxide nanoparticles coated with chitosan and gallic acid was 14 ± 3 nm (Figure 6D).

Release behavior of gallic acid

The release profiles for gallic acid from the FCG nanocarrier in aqueous solution of 0.0001 M Na_2CO_3 and phosphate-buff-

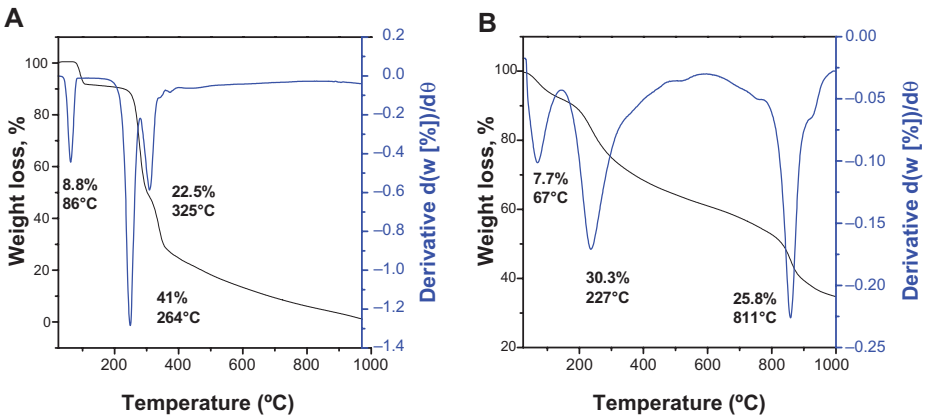

Figure 4 Thermogravimetric analysis of (**A**) gallic acid and (**B**) iron oxide nanoparticles coated with chitosan and gallic acid.

ered solution at pH levels of 7.4 and 4.8 are shown in Figure 7. The gallic acid release profiles from FCG into 0.0001 M Na_2CO_3 solution showed a fast release at the beginning, then 70% release during the first 150 minutes, followed by a slower step of 96.7% for the second 1200 minutes (Figure 7A). The fast initial release is presumably due to release of gallic acid anions from the nanocarrier structure, and the slower release is attributed to the exchange of gallic acid in the internal core-shell structure of the nanocarrier with anions in solution. Figures 7B and C show the release profiles for gallic acid into phosphate-buffered solution at pH 4.8 and 7.4, respectively. It is obvious that the release of gallic acid from

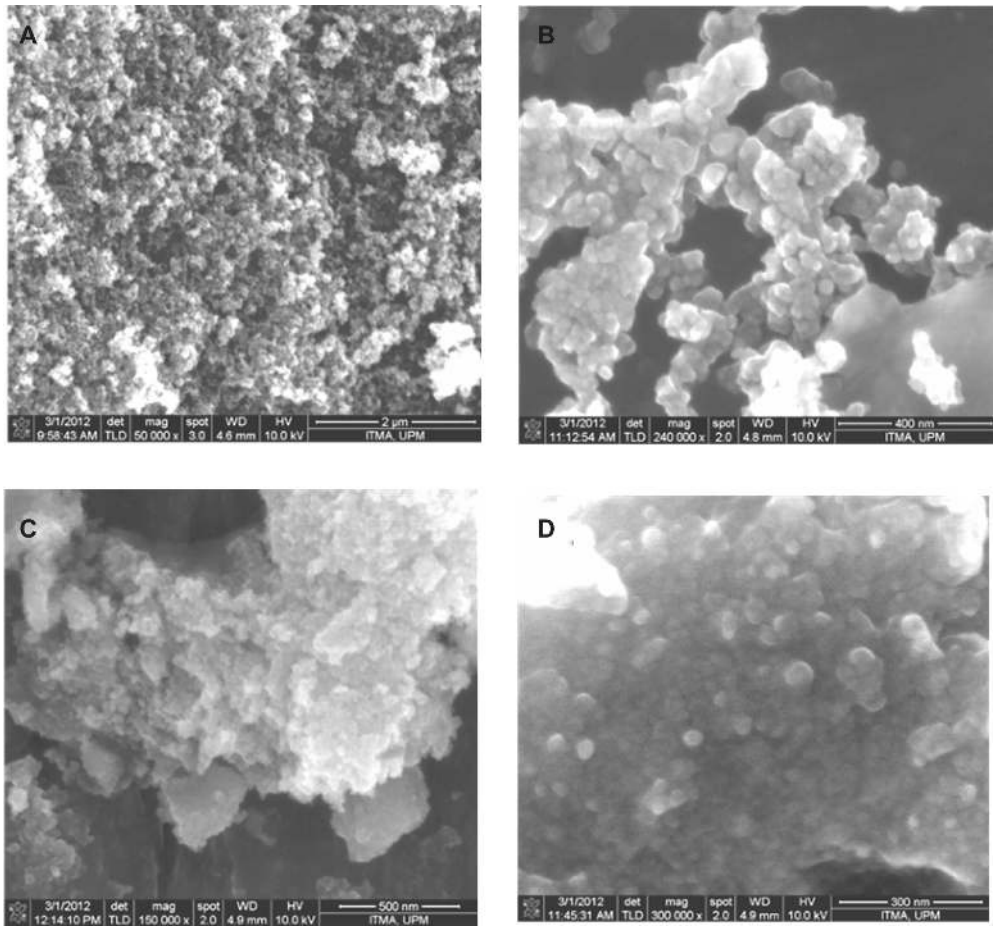

Figure 5 Field emission scanning electron microscopy images of (**A**) iron oxide magnetic nanoparticles at 50,000× magnifications, (**B**) iron oxide nanoparticles at 240,000× magnification, (**C**) iron oxide nanoparticles coated with chitosan and gallic acid at 150,000× magnification, and (**D**) iron oxide nanoparticles coated with chitosan and gallic acid at 300,000× magnification.

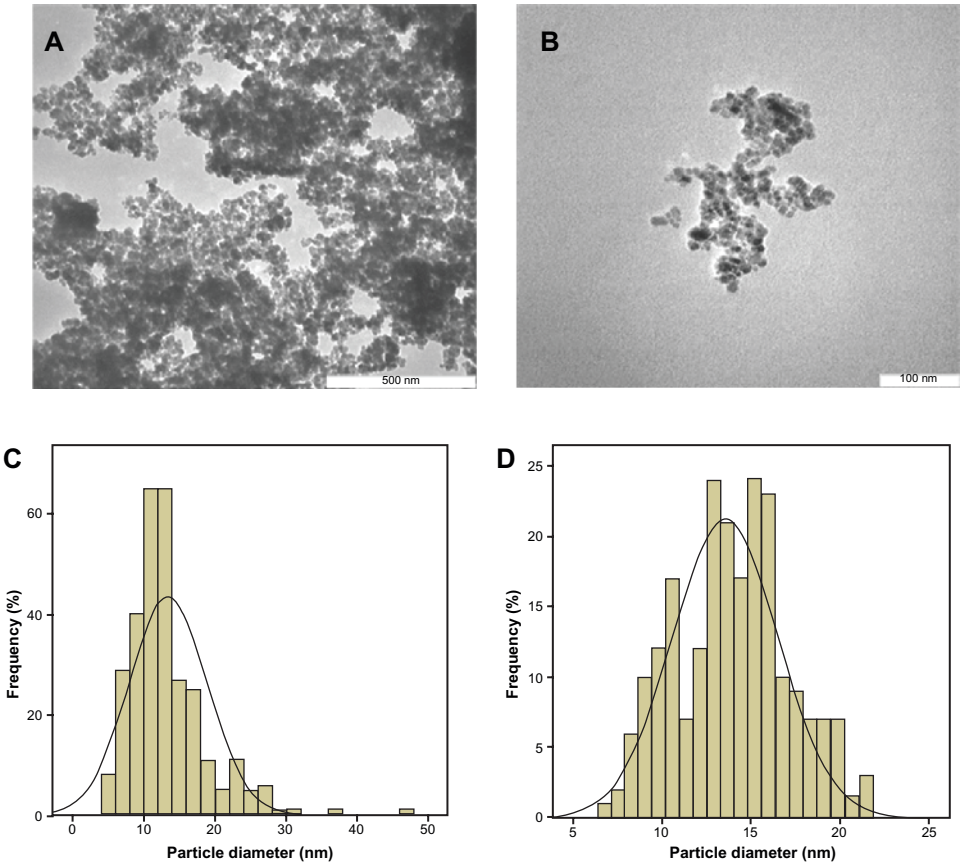

Figure 6 Transmission electron micrographs (**A**) for iron oxide magnetic nanoparticles with 500 nm bar, (**B**) iron oxide nanoparticles coated with chitosan and gallic acid with 100 nm magnetic bar, (**C**) particle diameter of iron oxide nanoparticles, and (**D**) particle diameter of iron oxide nanoparticles coated with chitosan and gallic acid.

the nanocarrier depends on pH, with the release rate at pH 7.4 being remarkably lower than that at pH 4.8. The amount of gallic acid released from the nanocarrier reached 90.8% within approximately 1300 minutes when exposed to the pH 4.8 solution. When the pH of the solution was changed to 7.4, the release rate of gallic acid decreased to 58.1%. The different release rates observed at pH 4.8 and pH 7.4 could possibly be due to the different release mechanism for gallic acid in the core-shell structure of the different nanocarriers. In addition, at pH 7.4, the FCG nanocarrier is more stable, and release would occur by an anion exchange process.

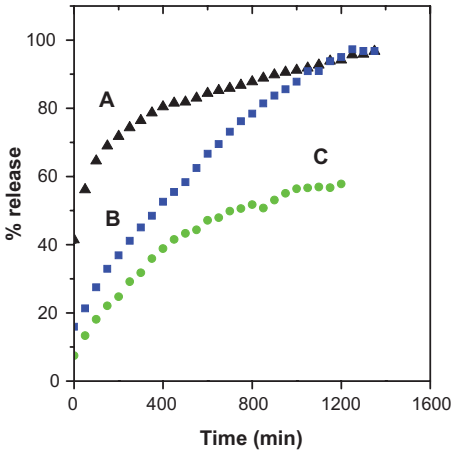

Figure 7 Release profiles of gallic acid from the iron oxide nanoparticles coated with chitosan and gallic acid into (**A**) aqueous solution of 0.0001 M Na_2CO_3, (**B**) phosphate-buffered solution at pH 4.8, and (**C**) at pH 7.4.

Release kinetics of gallic acid

In order to investigate the release kinetic behavior of gallic acid from the FCG nanocarrier, pseudo-first order (equation 1), pseudo-second order (equation 2), and a parabolic diffusion equation (equation 3) were studied.[46,47] The equations are shown below:

$$\mathrm{Ln}\,(q_e - q_t) = \ln q_e - k_1 t \quad (1)$$

$$t/q_t = 1/k_2 q_e^{\,2} + t/q_e \quad (2)$$

$$(1 - M_t/M_0)/t = kt^{-0.5} + b \quad (3)$$

The q_e and q_t are the equilibrium release amount and the release amount at time t, respectively; k is the constant of

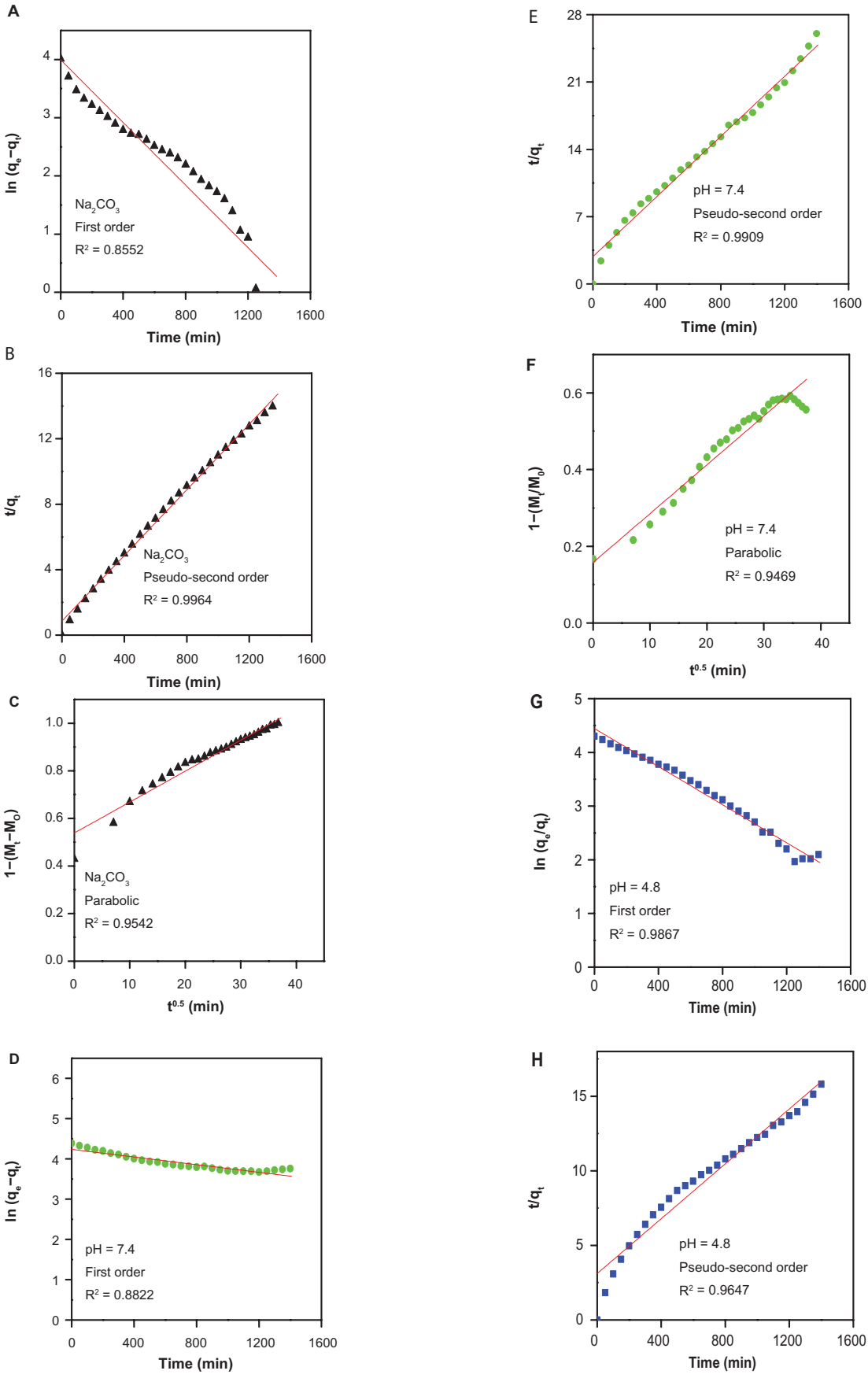

Figure 8 (*Continued*)

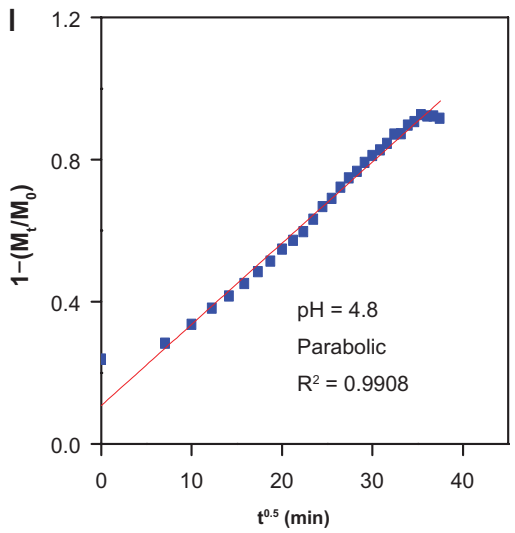

Figure 8 Fitting graphs for gallic acid release from iron oxide nanoparticles coated with chitosan and gallic acid, into different solutions to the first-order and pseudo-second order kinetics, and the parabolic equation for 0.0001 M Na_2CO_3 (**A**–**C**), pH 7.4 (**D**–**F**), and pH 4.8 (**G**–**I**).

the corresponding release rate; and M_0 and M_t represent the drug content remaining in the FCG nanocarrier at release times 0 and t, respectively.

On the basis of these three models (Figure 8 and Table 2), it can be seen that the pseudo-second order model can be better used to describe the gallic acid release behavior than the other models. Figure 8B shows that for Na_2CO_3 solution, a pseudo-second order can be better fitted to the data [correlation coefficient (R^2) and k values are 0.9964 and 1.18×10^{-4} mg per minute, respectively]. The same kinetic models were also applied to the phosphate-buffered solution at pH 7.4. Figure 8E shows a better fitted release profile at pH 7.4 using a second-order kinetics model (correlation coefficient of $R^2 = 0.9909$ and a rate constant of 8.63×10^{-5}). At pH 4.8, the release of gallic acid from FCG is consistent with a parabolic equation with a correlation coefficient of 0.9908. Table 2 shows the $t_{1/2}$ time release of gallic acid into aqueous solution of Na_2CO_3 and phosphate-buffered solution at pH 7.4 and 4.8, which was 85 minutes and 181 minutes, respectively (for second-order kinetics).

In vitro bioassay

The in vitro bioassay, as shown in Figure 9, tells us that, after 72 hours of treatment, neither gallic acid nor FCG was toxic to a normal human fibroblast (3T3) cell line tested using various doses (0.47, 0.94, 1.88, 3.75, 7.5, and 15.0 µg/mL) as indicated by the MTT result, whereas the cell viability of the treated well continued to rise with each increase in gallic acid or FCG concentration, reaching a value of 130% compared with control (untreated well, 100%). However, the same doses of gallic acid and FCG showed some toxicity to both MCF7 and HT29 cell lines, both of which are cancerous in nature, with cell viability decreasing to less than 30% at a gallic acid concentration of 7 µg/mL in both cell lines and to less than 80% at 15 µg/mL of FCG also on both cell lines, thus indicating the anticancer activity of gallic acid and FCG. Greater anticancer activity was seen in the HT29 cell line (Figure 9C) than in the MCF7 cell line (Figure 9B), and to the same extent with pristine gallic acid and FCG in both cell lines. Exposure to gallic acid and FCG produced a range of cytotoxicity responses in HT29 and MCF7 cell, but none was seen in the 3T3 cell line after 72 hours using the MTT assay (Figure 9A). Based on the study data, HT29 cells are more susceptible than MCF7 cells to nanoparticles containing gallic acid, although to a lesser degree than the effect seen in both cell lines using pristine gallic acid.

The toxicity shown only in cancer cells is in agreement with the anticancer properties shown by other researchers.[48,49] Differences in the toxic effect of gallic acid in different cancer cell lines is likely to be due to induction of cell death or cell cycle arrest in an apparently different manner by gallic acid.[48]

Conclusion

This study shows that the average size of magnetite prepared using ultrasonic irradiation is about 11 nm, compared with

Table 2 Correlation coefficient (R^2), rate constant (k), and half-time ($t_{1/2}$) obtained by fitting the data of the release of gallic acid from FCG into 0.0001 M Na_2CO_3 and in phosphate-buffered solution at pH 7.4 and 4.8

Aqueous Solution	Saturated release %	R^2			Rate constant (k) (mg/min)	$t_{1/2}$ (min)
		Pseudo-first order	Pseudo-second order	Parabolic diffusion		
Na_2CO_3	96.7	0.8552	0.9964	0.9542	$1.18 \times 10^{-4,a}$	85
pH 7.4	58.1	0.8822	0.9909	0.9469	$8.63 \times 10^{-5,b}$	181
pH 4.8	90.8	0.9867	0.9647	0.9908	$2.29 \times 10^{-2,c}$	150

Notes: [a,b]Estimated using pseudo-second order kinetics; [c]estimated using parabolic kinetics.
Abbreviations: GA, gallic acid; FCG, iron oxide nanoparticles coated with chitosan and gallic acid.

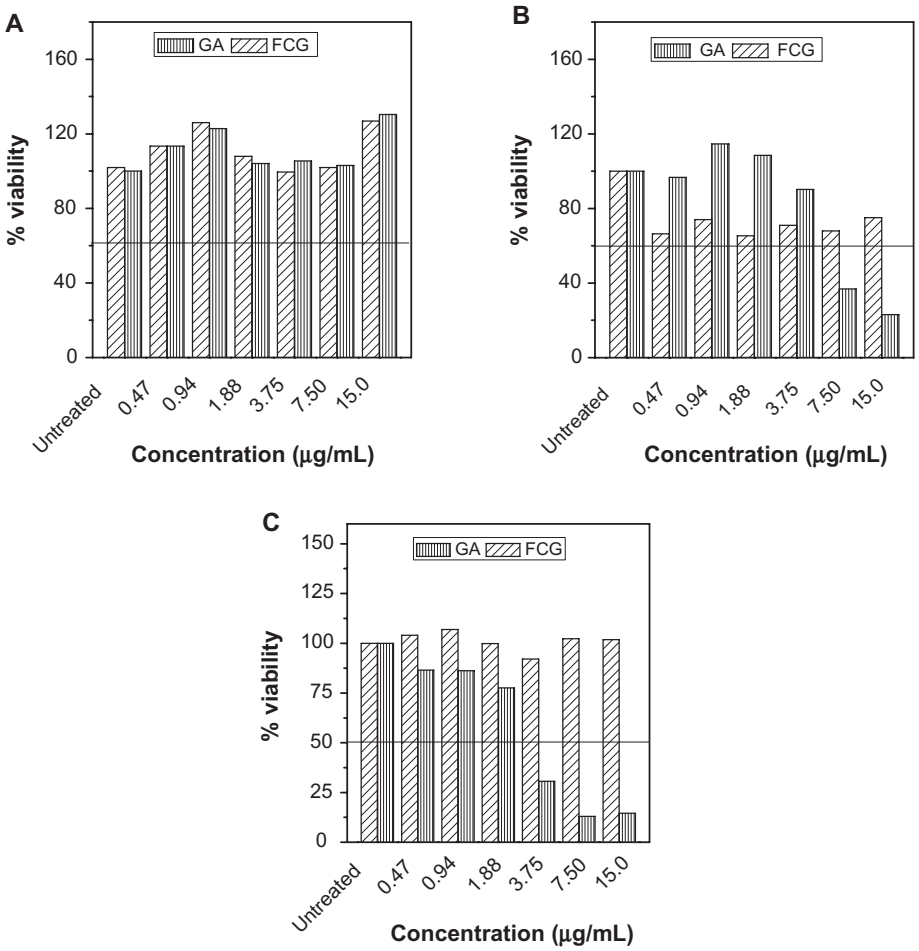

Figure 9 MTT assays of (**A**) normal human fibroblast (3T3) cell line, and anticancer activity in (**B**) MCF7, and (**C**) HT29 cell lines after 72 hours of treatment with gallic acid and iron oxide nanoparticles coated with chitosan and gallic acid at different concentrations.

13 nm after coating. The as-prepared superparamagnetic iron oxide was pure iron oxide with a cubic inverse spinel structure. Fourier transform infrared spectra showed that the iron oxide nanoparticles were successfully coated by chitosan and gallic acid. This controlled-release study shows that the release rate of gallic acid from FCG depends on the pH of the media and type of the host; when pH is 7.4, the release rate is slower than that at pH 4.8. It is also apparent that gallic acid was released in a controlled manner. In vitro bioassay results show that HT29 cells are more susceptible than MCF7 cells to nanoparticles containing gallic acid, although less than the effect shown using pristine gallic acid in both cell lines.

Acknowledgments

The authors are grateful to the Ministry of Science, Technology, and Innovation of Malaysia (MOSTI), for funding this project under National Nanotechnology Directorate, grant No. NND/NA/(1)/TD11-010, (UPM vot No. 5489100).

Disclosure

The authors report no conflicts of interest in this work.

References

1. Plank C, Schillinger U, Scherer F, et al. The magnetofection method: using magnetic force to enhance gene delivery. *Biol Chem*. 2005;384(5):737–747.
2. Sun Y, Duan L, Guo Z, et al. An improved way to prepare superparamagnetic magnetite-silica core-shell nanoparticles for possible biological application. *J Magn Magn Mater*. 2005;285(1):65–70.
3. Lu AH, Salabas EL, Schüth F. Magnetic nanoparticles: synthesis, protection, functionalization, and application. *Angew Chem Int Ed*. 2007;46(8):1222–1244.
4. Zubarev AY, Iskakova LY. To the theory of rheological properties of ferrofluids: influence of drop-like aggregates. *Physica A*. 2004;343:65–80.
5. Rossi LM, Silva FP, Vono LLR, et al. Superparamagnetic nanoparticle-supported palladium: a highly stable magnetically recoverable and reusable catalyst for hydrogenation reactions. *Green Chem*. 2007;9(4):379–385.
6. Lee JH, Jun Y, Yeon SI, Shin JS, Cheon J. Dual-mode nanoparticle probes for high-performance magnetic resonance and fluorescence imaging of neuroblastoma. *Angew Chem Int Ed Engl*. 2006;118(48):8340–8342.
7. Hu FQ, Wei L, Zhou Z, Ran YL, Li Z, Gao MY. Preparation of biocompatible magnetite nanocrystals for in vivo magnetic resonance detection of cancer. *Adv Mater*. 2006;18(19):2553–2556.

8. Nasongkla N, Bey E, Ren J, et al. Multifunctional polymeric micelles as cancer-targeted, MRI-ultrasensitive drug delivery systems. *Nano Lett*. 2006;6(11):2427–2430.
9. Wu W, He Q, Jiang C. Magnetic iron oxide nanoparticles: synthesis and surface functionalization strategies. *Nanoscale Res Lett*. 2008; 3(11):397–415.
10. Salehizadeh H, Hekmatian E, Sadeghi M, Kennedy K. Synthesis and characterization of core-shell Fe_3O_4-gold-chitosan nanostructure. *J Nanobiotechnol*. 2012;10(1):1–7.
11. Park HY, Schadt MJ, Wang L, et al. Fabrication of magnetic core@ shell Fe oxide@ Au nanoparticles for interfacial bioactivity and bio-separation. *Langmuir*. 2007;23(17):9050–9056.
12. Sonvico F, Mornet S, Vasseur S, et al. Folate-conjugated iron oxide nanoparticles for solid tumor targeting as potential specific magnetic hyperthermia mediators: synthesis, physicochemical characterization, and in vitro experiments. *Bioconjug Chem*. 2005;16(5): 1181–1188.
13. Zhang J, Misra RDK. Magnetic drug-targeting carrier encapsulated with thermosensitive smart polymer: Core-shell nanoparticle carrier and drug release response. *Acta Biomater*. 2007;3(6):838–850.
14. Jordan A, Scholz R, Maier-Hauff K, et al. Presentation of a new magnetic field therapy system for the treatment of human solid tumors with magnetic fluid hyperthermia. *J Magn Magn Mater*. 2001;225(1):118–126.
15. Fortin JP, Wilhelm C, Servais J, Ménager C, Bacri JC, Gazeau F. Size-sorted anionic iron oxide nanomagnets as colloidal mediators for magnetic hyperthermia. *J Am Chem Soc*. 2007;129(9): 2628–2635.
16. Silva AC, Oliveira TR, Mamani JB, et al. Application of hyperthermia induced by superparamagnetic iron oxide nanoparticles in glioma treatment. *Int J Nanomedicine*. 2011;6:591–603.
17. Johannsen M, Gneveckow U, Eckelt L, et al. Clinical hyperthermia of prostate cancer using magnetic nanoparticles: presentation of a new interstitial technique. *Int J Hyperthermia*. 2005;21(7):637–647.
18. Basel MT, Balivada S, Wang H, et al. Cell-delivered magnetic nanoparticles caused hyperthermia-mediated increased survival in a murine pancreatic cancer model. *Int J Nanomedicine*. 2012;7(1): 297–306.
19. Kuznetsov AA, Filippov VI, Alyautdin RN, Torshina NL, Kuznetsov OA. Application of magnetic liposomes for magnetically guided transport of muscle relaxants and anti-cancer photodynamic drugs. *J Magn Magn Mater*. 2001;225(1):95–100.
20. Kuznetsov AA, Filippov VI, Kuznetsov OA, Gerlivanov VG, Dobrinsky EK, Malashin SI. New ferro-carbon adsorbents for magnetically guided transport of anti-cancer drugs. *J Magn Magn Mater*. 1999;194(1): 22–30.
21. Moghimi SM, Hunter AC, Murray JC. Long-circulating and target-specific nanoparticles: theory to practice. *Pharmacol Rev*. 2001;53(2): 283–318.
22. Murdock RC, Braydich-Stolle L, Schrand AM, Schlager JJ, Hussain SM. Characterization of nanomaterial dispersion in solution prior to in vitro exposure using dynamic light scattering technique. *Toxicol Sci*. 2008;101(2):239–253.
23. Avilés MO, Ebner AD, Ritter JA. In vitro study of magnetic particle seeding for implant assisted-magnetic drug targeting. *J Magn Magn Mater*. 2008;320(21):2640–2646.
24. Zhou H, Yu W, Guo X, et al. Synthesis and characterization of amphiphilic glycidol- chitosan-deoxycholic acid nanoparticles as a drug carrier for doxorubicin. *Biomacromolecules*. 2010;11(12):3480–3486.
25. Gupta AK, Gupta M. Cytotoxicity suppression and cellular uptake enhancement of surface modified magnetic nanoparticles. *Biomaterials*. 2005;26(13):1565–1573.
26. Qu J, Liu G, Wang Y, Hong R. Preparation of Fe_3O_4-chitosan nanoparticles used for hyperthermia. *Adv Powder Technol*. 2010;21(4):461–467.
27. Pasanphan W, Chirachanchai S. Conjugation of gallic acid onto chitosan: an approach for green and water-based antioxidant. *Carbohydr Polym*. 2008;72(1):169–177.
28. Cho YS, Kim SK, Ahn CB, Je JY. Preparation, characterization, and antioxidant properties of gallic acid-grafted-chitosans. *Carbohydr Polym*. 2011;83(4):1617–1622.
29. Saifuddin N, Dinara S. Immobilization of Saccharomyces cerevisiae onto cross-linked chitosan coated with magnetic nanoparticles for adsorption of uranium (VI) ions. *Adv Nat Appl Sci*. 2012;6(2):249–267.
30. Feng J, Mao J, Wen X, Tu M. Ultrasonic-assisted in situ synthesis and characterization of superparamagnetic Fe_3O_4 nanoparticles. *J Alloys Compd*. 2011;509(37):9093–9097.
31. Andrade ÂL, Souza DM, Pereira MC, Fabris JD, Domingues RZ. pH effect on the synthesis of magnetite nanoparticles by the chemical reduction-precipitation method. *Química Nova*. 2010;33(3): 524–527.
32. Nakayama H, Hatakeyama A, Tsuhako M. Encapsulation of nucleotides and DNA into Mg-Al layered double hydroxide. *Int J Pharm*. 2010;393(1/2):105–112.
33. Wang Z, Wang E, Gao L, Xu L. Synthesis and properties of Mg_2Al layered double hydroxides containing 5-fluorouracil. *J Solid State Chem*. 2005;178(3):736–741.
34. Xia SJ, Ni ZM, Xu Q, Hu BX, Hu J. Layered double hydroxides as supports for intercalation and sustained release of antihypertensive drugs. *J Solid State Chem*. 2008;181(10):2610–2619.
35. Hussein MZ, Hashim N, Yahaya AH, Zainal Z. Synthesis and characterization of [4-(2, 4-dichlorophenoxybutyrate)-zinc layered hydroxide] nanohybrid. *Solid State Sci*. 2010;12(5):770–775.
36. Ribeiro C, Arizaga GGC, Wypych F, Sierakowski MR. Nanocomposites coated with xyloglucan for drug delivery: in vitro studies. *Int J Pharm*. 2009;367(1/2):204–210.
37. Hussein Al Ali SH, Al-Qubaisi M, Hussein MZ, Ismail M, Zainal Z, Hakim MN. Controlled release and angiotensin-converting enzyme inhibition properties of an antihypertensive drug based on a perindopril erbumine-layered double hydroxide nanocomposite. *Int J Nanomedicine*. 2012;7:2129–2141.
38. Hussein Al-Ali SH, Al-Qubaisi M, Hussein MZ, Ismail M, Zainal Z, Hakim MN. In vitro inhibition of histamine release behavior of cetirizine intercalated into Zn/Al-and Mg/Al-layered double hydroxides. *Int J Mol Sci*. 2012;13(5):5899–5916.
39. Hussein Al-Ali SH, Al-Qubaisi M, Hussein MZ, Zainal Z, Hakim MN. Preparation of hippurate-zinc layered hydroxide nanohybrid and its synergistic effect with tamoxifen on HepG2 cell lines. *Int J Nanomedicine*. 2011;6:3099–3111.
40. Hussein Al-Ali SH, Al-Qubaisi M, Hussein MZ, Ismail M, Zainal Z, Hakim MN. Comparative study of Mg/Al-and Zn/Al-layered double hydroxide-perindopril erbumine nanocomposites for inhibition of angiotensin-converting enzyme. *Int J Nanomedicine*. 2012;7:4251–4262.
41. Hussein Al-Ali SH, Al-Qubaisi M, et al. Controlled-release formulation of antihistamine based on cetirizine zinc-layered hydroxide nanocomposites and its effect on histamine release from basophilic leukemia (RBL-2H3) cells. *Int J Nanomedicine*. 2012;7:3351–3363.
42. Zhao Y, Qiu Z, Huang J. Preparation and analysis of magnetic Fe_3O_4 nanoparticles used as targeted-drug carriers. *Chinese J Chem Eng*. 2008;16(3):451–455.
43. Nidhin M, Indumathy R, Sreeram KJ, Nair BU. Synthesis of iron oxide nanoparticles of narrow size distribution on polysaccharide templates. *Bulletin of Materials Science*. 2008;31(1):93–96.
44. Ma H, Qi X, Maitani Y, Nagai T. Preparation and characterization of superparamagnetic iron oxide nanoparticles stabilized by alginate. *Int J Pharm*. 2007;333(1):177–186.
45. Ge Y, Zhang Y, Xia J, et al. Effect of surface charge and agglomerate degree of magnetic iron oxide nanoparticles on KB cellular uptake in vitro. *Colloid Surf B Biointerfaces*. 2009;73(2):294–301.
46. Dong L, Yan L, Hou WG, Liu SJ. Synthesis and release behavior of composites of camptothecin and layered double hydroxide. *J Solid State Chem*. 2010;183(8):1811–1816.
47. Ho YS, Ofomaja AE. Pseudo-second-order model for lead ion sorption from aqueous solutions onto palm kernel fiber. *J Hazard Mater*. 2006;129(1):137–142.

48. Fariedi A, Kurnia D, Faried LS, et al. Anticancer effects of gallic acid isolated from Indonesian herbal medicine, Phaleria macrocarpa (Scheff) Boerl, on human cancer cell lines. *Int J Oncol*. 2007;30(3):605–613.
49. Maurya DK, Nandakumar N, Devasagayam TPA. Anticancer property of gallic acid in A549, a human lung adenocarcinoma cell line, and possible mechanisms. *J Clin Biochem Nutr*. 2011;48(1):85–90.